J. Plasma Phys. (2020), *vol.* 86, 905860301
doi:10.1017/S0022377819000941

The onset of electron-only reconnection

Alfred Mallet†

Space Sciences Laboratory, University of California, Berkeley, CA 94720, USA

(Received 19 September 2019; revised 18 December 2019; accepted 19 December 2019)

Motivated by recent observations of 'electron-only' magnetic reconnection, without an ion-scale sheet or ion outflows, in both the Earth's magnetosheath and in numerical simulations, we study the formation and reconnection of electron-scale current sheets at low plasma β. We first show that ideal sheets collapse to thicknesses much smaller than the ion scales, by deriving an appropriate analogue of the Chapman–Kendall collapse solution. Second, we show that, in practice, reconnection onset happens in these collapsing sheets once they reach a critical aspect ratio, because the tearing instability then becomes faster than their collapse time scale. We show that this can happen for sheet thicknesses larger than the ion scale or at only a few times the electron scale, depending on plasma parameters and the aspect ratio of the collapsing structure, thereby unifying the usual picture of ion-coupled reconnection and the new regime of electron-only reconnection. We derive relationships between plasma β, ion-to-electron temperature ratio, the aspect ratio, electron outflow velocity and the final thickness of the sheets, and thus determine under what circumstances electron-scale sheets form and reconnect.

Key words: astrophysical plasmas, plasma nonlinear phenomena, space plasma physics

1. Introduction

Magnetic reconnection in current sheets is present in many astrophysical and laboratory settings and is an important process for converting magnetic energy into thermal and non-thermal kinetic energy (Zweibel & Yamada 2009; Ji *et al.* 2019; Yamada, Kulsrud & Ji 2010). In low-β collisionless guide-field reconnection, field lines are broken within a microscopic electron diffusion region, of size comparable to the electron inertial length $d_e = c/\omega_{pe}$, where $\omega_{pe} = \sqrt{4\pi n_e e^2/m_e}$ is the electron plasma frequency. In the usual picture of (guide-field) reconnection, this electron region is embedded in a larger-scale 'ion region' of thickness of order the ion sound scale $\rho_s = \rho_i\sqrt{ZT_e/2T_i}$, where the ion gyroradius $\rho_i = v_{\mathrm{th}i}/\Omega_i$, the ion thermal speed $v_{\mathrm{th}i} = \sqrt{2T_i/m_i}$ and the ion gyrofrequency $\Omega_i = ZeB_0/m_i c$. Associated with this region one expects bidirectional jets of plasma flowing away from the reconnection site at around the in-plane Alfvén speed $v_{\mathrm{A}y} = B_y/\sqrt{4\pi n_i m_i}$, where B_y is the reconnecting (in-plane) magnetic field. We will term this standard picture 'ion-coupled' reconnection.

However, recent analysis of data from the MMS spacecraft (Phan *et al.* 2018) has shown that, at least in Earth's turbulent magnetosheath, one overwhelmingly finds

† Email address for correspondence: alfred.mallet@berkeley.edu

current sheets with thicknesses of only a few d_e (i.e. much thinner than ρ_s) without associated ion regions and ion jets, but with clear electron jets moving at appreciable fractions of the electron Alfvén velocity $v_{Aey} = B_y/\sqrt{4\pi n_e m_e}$. This new regime has also recently been reproduced in the numerical simulations of Sharma Pyakurel *et al.* (2019). A similar situation has been observed in the hybrid Vlasov–Maxwell turbulence simulations of Califano *et al.* (2018), who observed that when energy is injected at scales much larger than the ion scales, ion-coupled reconnection is observed, while if energy is injected closer to the ion scales, only electron jets and electron-scale sheets are observed. Reconnection of current sheets with thicknesses of a few d_e is also observed in the VINETA-II experiment (Jain *et al.* 2017). We will follow the terminology of Califano *et al.* (2018) and term this new regime 'electron-only' reconnection.

The goal of this paper is to develop a theoretical picture that can explain the onset of this new regime of electron-only reconnection, and under what circumstances it occurs in place of the standard ion-coupled reconnection. To achieve this, we will make use of a simplified model, rigorously derived from gyrokinetics in the limit $\beta_e \sim m_e/m_i \ll 1$, the so-called 'kinetic reduced electron heating model', henceforth KREHM (Zocco & Schekochihin 2011). The details of this model, as well as its utility and limitations, are described in § 2.

To make progress in understanding electron-only reconnection onset, there are two main questions which should be answered. First, can current sheets collapse to thicknesses of order a few d_e, significantly below the ion scales? We answer this in § 3 by deriving a collapsing X-point solution analogous to Chapman–Kendall collapse (Chapman & Kendall 1963; Biskamp 2000), and showing that the solution is valid both above and below the ion scales. This means that ideal (i.e. with field lines frozen into an effective electron flow) sheets can indeed collapse well past the ion scale.

Second, at what sheet thickness do these collapsing sheets begin to reconnect, and under what conditions is this thickness above (obtaining ion-coupled reconnection) or well below (obtaining electron-only reconnection) the ion scales? We answer this in § 4, showing that the sheets are disrupted when they collapse to a critical thickness[1] at which the linear tearing growth rate[2] is faster than the collapse or formation rate of the sheet derived in § 3. Our analysis allows us to derive relationships between β_e and the aspect ratio and thickness of the sheet at disruption (reconnection onset), and we thus determine the physical conditions under which one will observe ion-coupled or electron-only reconnection. The essential physical result is that if the initial collapsing solution is not sufficiently anisotropic when its thickness is above the ion scales, the collapse continues down to a thickness well below the ion scale, and electron-only reconnection will occur. Remarkably (considering the formal limitation of KREHM to low β), we will see that our model seems to agree rather well with the magnetosheath observations of electron-only reconnection (Phan *et al.* 2018; Stawarz *et al.* 2019).

2. Equations

Our starting point is the KREHM derived by Zocco & Schekochihin (2011) (henceforth ZS11) from gyrokinetics for electron β of order the mass ratio $\beta_e \sim Zm_e/m_i$, where $Z = q_i/e$ (and the temperature ratio $\tau = T_{0i}/T_{0e} \sim 1$). The spatial scales

[1] Notably, this critical thickness at which reconnection onset occurs is always larger than that of the steady-state reconnecting configuration, derived in appendix A, similar to the results of Pucci & Velli (2014) and Uzdensky & Loureiro (2016) for resistive reconnection onset.

[2] We derive the growth rate of the tearing mode for sheets with thicknesses below the ion scales in appendix B.

https://doi.org/10.1017/S0022377819000941 Published online by Cambridge University Press

of the fluctuations are ordered to be comparable to the relevant ion kinetic scales, $k_\perp \rho_i \sim k_\perp \rho_s \sim 1$, and so KREHM is able to capture both the large-scale ($k_\perp \rho_s \ll 1$) and small-scale ($k_\perp \rho_s \gg 1$) behaviour of the plasma, as well as the transition between them. This is essential for our present purposes, since we are attempting to diagnose the transition between ion-coupled and electron-only reconnection onset.

KREHM is in some sense a minimal model for describing collisionless guide-field reconnection, since the equations incorporate the dispersive effects entering at the ion sound scale ρ_s that are thought to be essential to enable fast reconnection (Rogers *et al.* 2001), a flux-unfreezing mechanism (electron inertia) entering at the electron inertial scale d_e, and a rigorous treatment of the (electron) heating channel. The equations, written in terms of the electrostatic potential ϕ, the magnetic potential $A_\parallel$ and the reduced electron distribution function g_e, are

$$\frac{\mathrm{d}}{\mathrm{d}t}\frac{Z}{\tau}(1-\hat{\Gamma}_0)\frac{e\phi}{T_{0e}} = \hat{\boldsymbol{b}}\cdot\boldsymbol{\nabla}\frac{e}{cm_e}d_e^2\nabla_\perp^2 A_\parallel, \tag{2.1}$$

$$\frac{\mathrm{d}}{\mathrm{d}t}(A_\parallel - d_e^2\nabla_\perp^2 A_\parallel) = -c\frac{\partial\phi}{\partial z} - \frac{cT_{0e}}{e}\hat{\boldsymbol{b}}\cdot\boldsymbol{\nabla}\left[\frac{Z}{\tau}\left(1-\hat{\Gamma}_0\right)\frac{e\phi}{T_{0e}} - \frac{\delta T_{\parallel e}}{T_{0e}}\right], \tag{2.2}$$

$$\frac{\mathrm{d}g_e}{\mathrm{d}t} + v_\parallel\hat{\boldsymbol{b}}\cdot\boldsymbol{\nabla}\left(g_e - \frac{\delta T_{\parallel e}}{T_{0e}}F_{0\mathrm{e}}\right) = C[g_e] + \left(1-\frac{2v_\parallel^2}{v_{\mathrm{the}}^2}\right)F_{0\mathrm{e}}\hat{\boldsymbol{b}}\cdot\boldsymbol{\nabla}\frac{e}{cm_e}d_e^2\nabla_\perp^2 A_\parallel, \tag{2.3}$$

where

$$\frac{\mathrm{d}}{\mathrm{d}t} = \frac{\partial}{\partial t} + \frac{c}{B_0}\{\phi, \ldots\}, \tag{2.4}$$

$$\hat{\boldsymbol{b}}\cdot\boldsymbol{\nabla} = \frac{\partial}{\partial z} - \frac{1}{B_0}\{A_\parallel, \ldots\}, \tag{2.5}$$

$$\frac{\delta T_{\parallel e}}{T_{0e}} = \frac{1}{n_{0\mathrm{e}}}\int d^3\boldsymbol{v}\frac{2v_\parallel^2}{v_{\mathrm{the}}^2}g_e, \tag{2.6}$$

and $\hat{\Gamma}_0$, encoding the ion finite Larmor radius effects, is the inverse Fourier transform of

$$\Gamma_0\left(\tfrac{1}{2}k_\perp^2\rho_i^2\right) = \mathrm{I}_0\left(\tfrac{1}{2}k_\perp^2\rho_i^2\right)\mathrm{e}^{-1/2k_\perp^2\rho_i^2}, \tag{2.7}$$

where I_0 is the modified Bessel function. The electron density perturbation δn_e is related to ϕ via the relation

$$\frac{\delta n_e}{n_{0e}} = -\frac{Z}{\tau}\left(1-\hat{\Gamma}_0\right)\frac{e\phi}{T_{0e}}. \tag{2.8}$$

The Poisson bracket appearing in the equations is $\{f, g\} = \hat{\boldsymbol{z}}\cdot\boldsymbol{\nabla}_\perp f\times\boldsymbol{\nabla}_\perp g$. We have taken the limit $\nu_{ei} \ll \omega$, which allows us to neglect a resistive term in (2.2) (but not the collisions $C[g_e]$ in (2.3)).

The function g_e is a mathematically convenient reduced electron-gyrocentre parallel velocity distribution function, which encodes the electron heating channel. This is perhaps all the information that is needed to understand the present paper: in more detail, it is related to the perturbed distribution function δf_e by

$$\delta f_e(\boldsymbol{r}, \boldsymbol{v}, t) = \left(1 + \frac{\delta n_e}{n_{0e}} + \frac{2v_\parallel u_{\parallel e}}{v_{\mathrm{the}}^2}\right)F_{0e} + g_e(\boldsymbol{R}_e, \boldsymbol{v}, t), \tag{2.9}$$

where $\boldsymbol{R}_e = \boldsymbol{r} + \boldsymbol{v}_\perp\times\hat{\boldsymbol{z}}/\Omega_e$ is the electron gyrocentre. Integrating the zeroth and first $v_\parallel$-moments of δf_e over all velocity (perturbed electron density and parallel flow),

https://doi.org/10.1017/S0022377819000941 Published online by Cambridge University Press

we can see that contribution from g_e to these vanishes, i.e. g_e contains the information of all higher moments, but not density or parallel flow. It turns out (see ZS11 for details) that the non-trivial $v_\perp$ dependence of g_e can be safely ignored, and so g_e can be considered a function of $v_\parallel$, space and time only.

We may write (2.2) as

$$\frac{\partial A_\parallel}{\partial t} = -c\hat{\boldsymbol{b}} \cdot \boldsymbol{\nabla} \left[\phi + \frac{Z}{\tau} \left(1 - \hat{\Gamma}_0 \right) \phi - \frac{\delta T_{\parallel e}}{e} \right] + \frac{\mathrm{d}}{\mathrm{d}t} d_e^2 \boldsymbol{\nabla}_\perp^2 A_\parallel, \tag{2.10}$$

which defines an effective velocity

$$\boldsymbol{u}_{\mathrm{eff}} = \hat{z} \times \boldsymbol{\nabla}_\perp \frac{c}{B_0} \left[\phi + \frac{Z}{\tau} \left(1 - \hat{\Gamma}_0 \right) \phi - \frac{\delta T_{\parallel e}}{e} \right], \tag{2.11}$$

into which the field lines are frozen, apart from the effects of electron inertia (Zocco & Schekochihin 2011). Thus, field lines are only broken when gradients are of order d_e^{-1}.

These equations have various interesting limits. First, for fluctuations on long length scales (compared to the ion gyroradius) $k_\perp \rho_i \ll 1$, and $\Gamma_0 \approx 1 - k_\perp^2 \rho_i^2/2$, and one can show that the equations reduce to those of RMHD, reduced magnetohydrodynamics (Strauss 1976), describing nonlinearly interacting Alfvénic fluctuations propagating up and down the magnetic field. Second, if one takes $k_\perp \rho_i \gg 1$, $\Gamma_0 \approx 0$, and subsequently expand in the square root of the mass ratio $\sqrt{m_e/m_i}$, i.e. $k_\perp d_e \ll 1$, one obtains the equations of ERMHD, electron reduced magnetohydrodynamics (Schekochihin *et al.* 2009), which involve nonlinearly interacting kinetic-Alfvén fluctuations propagating up and down the field.

It is important to note that, as mentioned earlier, formally these equations are only valid for $\beta_i \sim \beta_e \ll 1$. This rather limits their formal applicability to some physical regimes, including the magnetosheath, where electron-only reconnection has recently been observed (Phan *et al.* 2018; Stawarz *et al.* 2019), where $\beta_i \gtrsim 1$ and $\beta_e \lesssim 1$. Nonetheless, we believe that their simplicity allows us to model the essential physics of current sheet collapse and reconnection onset in a useful way, for three main reasons. First, simulations of turbulence using KREHM have revealed that it seems to compare rather well with more complete models, even at higher β than its formal regime of applicability (Grošelj *et al.* 2017). Second, we will show in § 3 that the Chapman–Kendall-like current sheet collapse solution also exists in ERMHD at arbitrary β_i and τ, meaning that this part of the analysis remains true even without the formal $\beta_i \ll 1$ requirement. Finally, the collisionless tearing mode (which we will show enables the onset of reconnection in § 4) has a growth rate that decreases with β_e (Numata & Loureiro 2015) for constant ratio of sheet thickness to ρ_i, meaning that at higher β_e, the basic physics of our picture will remain, but with the sheets potentially attaining even smaller (relative to ρ_i) thicknesses.

We should also mention here that Boldyrev & Loureiro (2019) have used a set of fluid equations derived for $k_\perp \rho_i \gg 1$, $\beta_i \sim 1$, $\beta_e \ll 1$ to study the small-scale tearing instability and its effect on turbulence, obtaining some results similar to ours (which is an additional source of reassurance that our low-β_i ordering does not invalidate the basic picture of tearing-induced reconnection onset): we have used KREHM instead because, first, we want a set of equations covering the ion-scale transition at $k_\perp \rho_i \sim 1$ to describe the transition between the ion-coupled and electron-only reconnection regimes, and second, the electron heating channel as encoded by (2.3) is important for a realistic picture of reconnection.

https://doi.org/10.1017/S0022377819000941 Published online by Cambridge University Press

3. X-point collapse

For electron-only reconnection to occur, it must first be possible to form current sheets with thicknesses well below the ion scale. In ideal MHD (magnetohydrodynamics), it is well known that X-points tend to collapse into sheets (Syrovatskii 1981). It turns out that this is still true in our system of equations, even at scales well below the ion gyroradius. If we require

$$\hat{\boldsymbol{b}} \cdot \boldsymbol{\nabla} \nabla_{\perp}^2 A_{\parallel} = 0, \tag{3.1}$$

then $g_e = 0$ is a solution. Let us also impose a 'vorticity-free' condition on the system,

$$\nabla_{\perp}^2 \phi = 0. \tag{3.2}$$

Under this condition, $\hat{\Gamma}_0 \phi = \phi$[3], and along with (3.1), the whole of (2.1) vanishes. Our flow must, of course, be consistent with maintaining the condition (3.1).

3.1. *Chapman–Kendall solution*

One (two-dimensional) solution which satisfies the conditions (3.1), (3.2) is a slightly modified version of 'Chapman–Kendall' collapse (Chapman & Kendall 1963; Biskamp 2000), originally derived for MHD (but which turns out to still be applicable here),

$$\phi = \frac{B_0}{c} \frac{\Lambda(t)}{2} xy, \tag{3.3}$$

$$A_{\parallel} = \frac{B_{\perp}}{2} \left(\frac{x^2 + 2d_e^2}{a(t)} - \frac{y^2 + 2d_e^2}{L(t)} \right), \tag{3.4}$$

where $a(t)$ and $L(t)$ are the thickness and length of the current sheet respectively. This solution is an approximation valid in the region close to the X-point in the interior of a realistic current sheet. Inserting this into (2.10), we obtain

$$\dot{a} = -\Lambda(t) a, \tag{3.5}$$

$$\dot{L} = \Lambda(t) L. \tag{3.6}$$

Thus, in the absence of reconnection, current sheets can thin to scales much smaller than the ion scales. However, this does not show that such thin sheets are always physically realisable: we will show in § 4 that, in fact, localised current configurations with $L > a$ are disrupted by the onset of reconnection at scales larger than d_e (but, importantly, sometimes smaller than ρ_s)[4]. White, Hazeltine & Loureiro (2018) have found that KREHM also allows a more general class of Chapman–Kendall-like solutions, for example a helically twisted version of the simple solution presented here.

[3]The series defining the modified Bessel function is $\mathrm{I}_0(x) = \sum_{m=0}^{\infty} (x/2)^{2m}/(m!)^2$, so $\hat{\Gamma}_0$ is just a series in $\nabla_{\perp}^2$, with the $m = 0$ term being 1. If we had first taken the small-scale limit $k_{\perp}\rho_i \gg 1$ and said that $\hat{\Gamma}_0 \approx 0$ using the large-argument asymptotic expansion of I_0, we would have missed this fact.

[4]Indeed, equations (3.3), (3.4) are valid even at scales below d_e: perhaps a hint that something interesting might happen at a larger scale which invalidates this simple scenario.

https://doi.org/10.1017/S0022377819000941 Published online by Cambridge University Press

3.2. *Choosing* $\Lambda(t)$

It remains for us to decide a reasonable form for $\Lambda(t)$. We do this in two limiting cases, $a \gg \rho_i$ and $a \ll \rho_i$, and ask that the outflows match the characteristic wave speed involved in maintaining the structure of the sheet in the y-direction in both cases. In the case where $a \gg \rho_i$, the outflows should attain the constant in-plane Alfvén speed $v_{\mathrm{A}y} = B_y(a)/\sqrt{4\pi n_{0i} m_i}$ at $y \sim L(t)$. In the small-scale case where $a \ll \rho_i$, the outflow speed at $y \sim L(t)$ should be the in-plane kinetic-Alfvén wave speed (see ZS11 or Schekochihin *et al.* 2009),

$$u_{\mathrm{KAW}y} = \sqrt{\frac{1}{2}\left(1+\frac{Z}{\tau}\right)}\, v_{\mathrm{A}y}\frac{\rho_i}{a(t)}. \tag{3.7}$$

Importantly, this is inversely proportional to a. Thus, it is physically reasonable to choose

$$\Lambda(t) = \begin{cases} \dfrac{2v_{\mathrm{A}y}}{L(t)}, & a \gg \rho_i, \\ \dfrac{\sqrt{2(1+Z/\tau)}\, v_{\mathrm{A}y}\rho_i}{a(t)L(t)}, & a \ll \rho_i, \end{cases} \tag{3.8}$$

which defines (inverse) time scales associated with forming sheets of thickness a and length L. With these choices, equations (3.5) and (3.6) have the solutions

$$a \gg \rho_i: \quad L = L_0 + 2v_{\mathrm{A}y}t, \quad a = a_0L_0/L, \tag{3.9}$$

$$a \ll \rho_i: \quad L = L_0 \exp\left(\frac{\sqrt{2(1+Z/\tau)}\, v_{\mathrm{A}y}\rho_i}{a_0L_0}t\right), \quad a = a_0L_0/L. \tag{3.10}$$

The aspect ratio as a function of a is given by

$$\frac{L}{a} = \frac{a_0L_0}{a^2}, \tag{3.11}$$

simply from continuity. It is important to note that, if the sheets are formed as part of turbulence, this scaling is not accurate, because structures will interact with each other as well as undergoing their own nonlinear evolution. Instead, one might expect, for $a \gg \rho_i$, $L/a \propto a^{-1/4}$ (cf. Boldyrev 2006; Chandran, Schekochihin & Mallet 2015; Mallet & Schekochihin 2017). The aspect ratio scaling for $a \ll \rho_i$ in turbulence is as yet unknown.

3.3. *Collapse time*

Let us start with a structure of thickness $a_0 > \rho_i$, and ask how long it takes for it to collapse to a thickness $a_* < \rho_i$. First, using (3.9), the time taken to collapse to ρ_i is

$$t_\rho \sim \left(\frac{a_0}{\rho_i} - 1\right)\frac{L_0}{2v_{\mathrm{A}y}} \approx \frac{a_0L_0}{2v_{\mathrm{A}y}\rho_i}. \tag{3.12}$$

Subsequent collapse from ρ_i down to a_* occurs according to (3.10) in a time

$$t_* \sim \frac{a_0L_0\ln(\rho_i/a_*)}{\sqrt{2\left(1+\frac{Z}{\tau}\right)}\, v_{\mathrm{A}y}\rho_i}, \tag{3.13}$$

which is, in practice, usually of order t_ρ. Thus, the total collapse time is of order t_ρ, and mainly depends on the initial size and reconnecting field within the structure.

https://doi.org/10.1017/S0022377819000941 Published online by Cambridge University Press

3.4. *Current sheet collapse at higher β*

Finally, the question of whether or not this collapse process depends crucially on the low-β ordering used to derive KREHM may be of interest to the reader. First, for $k_\perp \rho_i \ll 1$, the Chapman–Kendall collapse obviously works, since the RMHD equations are valid at arbitrary β and can be derived from gyrokinetics under the assumption $k_\perp \rho_i \ll 1$ (Schekochihin *et al.* 2009). Second, for $k_\perp \rho_i \gg 1$, we can examine the (two-dimensional) electron reduced MHD equations (Schekochihin *et al.* 2009), which may be manipulated into the following form, chosen for their similarity to (2.1) and (2.2),

$$\frac{\mathrm{d}}{\mathrm{d}t}\frac{Z}{\tau}\frac{e\phi}{T_{0e}} = \frac{2}{2+\beta_i\left(1+\dfrac{Z}{\tau}\right)}\hat{\boldsymbol{b}}\cdot\boldsymbol{\nabla}\frac{e}{cm_e}d_e^2\boldsymbol{\nabla}_\perp^2 A_\parallel, \tag{3.14}$$

$$\frac{\mathrm{d}}{\mathrm{d}t}A_\parallel = -\frac{cT_{0e}}{e}\hat{\boldsymbol{b}}\cdot\boldsymbol{\nabla}\left[\frac{Z}{\tau}\frac{e\phi}{T_{0e}}\right]. \tag{3.15}$$

The effective velocity into which the field lines are frozen is

$$\boldsymbol{u}_{\mathrm{eff}} = \hat{z}\times\boldsymbol{\nabla}_\perp\frac{c}{B_0}\left(1+\frac{Z}{\tau}\right)\phi, \tag{3.16}$$

which can be compared with (2.11). Under the condition (3.1), equation (3.14) vanishes[5]. Inserting (3.3) and (3.4) with $d_e = 0$ into (3.15), and requiring the outflow velocity to be the in-plane kinetic-Alfvén velocity (at larger β_i, see Schekochihin *et al.* 2009),

$$u_{\mathrm{KAW}y} = \sqrt{\frac{1+Z/\tau}{2+\beta_i(1+Z/\tau)}}v_{\mathrm{A}y}\frac{\rho_i}{a(t)}, \tag{3.17}$$

we find that the solutions for $a(t)$ and $L(t)$ are

$$L = L_0\exp\left(\frac{\sqrt{\dfrac{2(1+Z/\tau)}{1+\beta_i(1+Z/\tau)/2}}v_{\mathrm{A}y}\rho_i}{a_0L_0}t\right), \quad a = a_0L_0/L, \tag{3.18a,b}$$

only mildly different to the KREHM case. Thus, the fact that current sheets collapse even at thicknesses $a \ll \rho_i$ does not depend on the $\beta \ll 1$ ordering of KREHM.

4. Disruption of forming sheets by the tearing instability

A useful model of the disruption of forming current sheets by reconnection has been developed recently by Uzdensky & Loureiro (2016). In this model, collapsing sheets are disrupted if their linear tearing mode is faster than their formation time scale, i.e.

$$\gamma/\Lambda(t) > 1, \tag{4.1}$$

assuming that the nonlinear stage of the tearing mode is at least as fast as the linear stage.

In general, the tearing mode that disrupts the sheet has the maximum tearing growth rate $\gamma_{\max}$ if it fits into the sheet, i.e. if $k_{\max}L > 1$, and by the growth rate of the longest-wavelength mode that fits in the sheet otherwise, i.e. the mode with $k_yL = 1$. The relevant tearing growth rates for our system are summarised in table 1: the growth rates for the case $a \gg \rho_s$ are derived in ZS11, while we derive the growth rates for the opposite case with $a \ll \rho_s$ in appendix B.

[5]Note that the $\mathrm{d}\phi/\mathrm{d}t$ in (3.14) could in fact just be written $\partial\phi/\partial t$, because $\{\phi,\phi\} = 0$.

https://doi.org/10.1017/S0022377819000941 Published online by Cambridge University Press

a/ρ_s	$\Delta'\delta_{\rm in}$	$\gamma/k_y v_{\rm Ay}$	δ	$\delta_{\rm in}$	$\gamma_{\max}a/v_{\rm Ay}$	$k_{\max}a$
$\gg 1$	$\ll 1$	$H\Delta' d_e\rho_s/a$	$Hd_e^2\Delta'$	$H^{1/2}d_e\rho_s^{1/2}\Delta'^{1/2}$	$\dfrac{Hd_e^{1/3+2/3n}\rho_s^{2/3+1/3n}}{a^{1+1/n}}$	$\left(\dfrac{d_e^{2/3}\rho_s^{1/3}}{a}\right)^{1/n}$
	$\gg 1$	$H\rho_s^{2/3}d_e^{1/3}/a$	$Hd_e^{4/3}\rho_s^{-1/3}$	$H^{1/2}\rho_s^{1/3}d_e^{2/3}$		
$\ll 1$	$\ll 1$	$H\Delta' d_e\rho_s/a$	$Hd_e^2\Delta'$	δ	$\dfrac{H\rho_s}{a}\left(\dfrac{d_e}{a}\right)^{1/n}$	$\left(\dfrac{d_e}{a}\right)^{1/n}$
	($\gg 1$	$H\rho_s/a$	Hd_e	δ)		

TABLE 1. Scalings for the collisionless tearing mode in various limits, as discussed in appendix B. The final row, $a/\rho_s \ll 1$ and $\Delta'\delta_{\rm in} \gg 1$, is probably inaccurate since we do not have an analytic solution. The quantity $H = \sqrt{1+\tau/Z}$; please see the appendix for details.

4.1. *Critical aspect ratio*

One can show that for our choice of $\Lambda(t)$, in the case $a \gg \rho_s$, $k_{\max}$ becomes accessible before the mode with $k_y L = 1$ goes unstable, while in the case where $a \ll \rho_s$, the sheet is disrupted when $k_{\max}L \sim 1$, and thus in practice we may always use $\gamma_{\max}$. Using (4.1), we find that sheets are disrupted for aspect ratios

$$\frac{L}{a} > \left(\frac{L}{a}\right)_{\rm crit} \sim \begin{cases} \dfrac{1}{\sqrt{1+\tau/Z}}\left(\dfrac{a}{d_e}\right)^{1/n}\left(\dfrac{a}{\rho_s}\right)\left(\dfrac{\rho_s}{d_e}\right)^{(1-1/n)/3}, & a \gg \rho_s \\ \left(\dfrac{a}{d_e}\right)^{1/n}, & a \ll \rho_s. \end{cases} \tag{4.2}$$

The $a \gg \rho_s$ expression was previously found by Del Sarto *et al.* (2016)[6].

We have shown that there is a maximum achievable aspect ratio for sheets with both $a \gg \rho_s$ and $a \ll \rho_s$. Inserting $a \sim \rho_s$ into (4.2), sheets will become unstable before they reach the ion scales ($a \sim \rho_s$) only if their aspect ratio becomes larger than $(\rho_s/d_e)^\nu$, where $1/n \leqslant \nu \leqslant 1/3 + 2/3n$. Once the sheet reaches the thickness at which it disrupts, it reconnects at that thickness[7] until all the available flux has been used up. Thus, if one observes a reconnecting (i.e. disrupting) sheet with length

$$L > \frac{\rho_s}{\sqrt{1+\tau/Z}}\left(\frac{m_e}{m_i}\frac{Z}{\beta_e}\right)^{\nu/2}, \tag{4.3}$$

one expects to see that the sheet thickness is larger than the ion scale and that there should be bidirectional ion jets moving at $v_{\rm Ay}$. This roughly agrees with the numerical simulations of Sharma Pyakurel *et al.* (2019), who found that to obtain fully ion-coupled guide-field reconnection, L needed to be of order $10d_i$, and is reminiscent of the results of Mandt, Denton & Drake (1994) for reconnection without a guide field, who observed a change in the scaling of the reconnection rate once the length of sheets became comparable to a few times the ion inertial length. In the magnetosheath interval studied by Phan *et al.* (2018) and subsequently Stawarz *et al.* (2019), $\beta_e \approx 0.5$ and $\tau/Z \approx 10$; choosing $\nu = 1$ and using the $a \gg \rho_s$ expression gives the critical length

[6]The expressions do not match for $a = \rho_s$: this is because the analysis of previous sections fails around $a \sim \rho_s$, where the operator $\hat{\Gamma}_0$ cannot be expanded in small or large argument.

[7]As in the picture of 'ideal tearing' proposed by Pucci & Velli (2014) and elaborated in e.g. Tenerani *et al.* (2016) for resistive reconnection.

https://doi.org/10.1017/S0022377819000941 Published online by Cambridge University Press

for ion-coupled reconnection $L/\rho_s \approx 10$ (this is also effectively the critical aspect ratio of such ion-coupled reconnecting sheets, since it is the point at which $a \approx \rho_s$). In other words, the fact that ion-scale sheets and ion jets are not often observed in the magnetosheath means that the aspect ratios of the sheets formed (presumably by the turbulent dynamics) are not extremely high.

As $a \to d_e$, current sheets of any appreciable aspect ratio greater than 1 are disrupted – so in practice, as one might have expected, the steady-state Sweet–Parker-like configuration, with width d_e (which we derive in appendix A) is not accessible. Reconnecting sheets for $a \ll \rho_s$ should have the aspect ratio given by the second expression in (4.2), and so we can estimate the aspect ratio of the sheets observed by Phan *et al.* (2018), with thicknesses $a \approx 4d_e$, to be no more than ≈ 4, using the $n = 1$ expression.

A simple estimate of the disruption time scale of the current sheets observed by Phan *et al.* (2018) is possible using (3.13). Given that aL is constant during collapse, we can estimate $a_0 L_0 = aL \approx 64 d_e^2$. Using $d_e \approx 1$ km, $v_{\mathrm{A}y} \approx 25$ kms^{-1} and $\rho_i \approx 100$ km, $t_* \approx 0.06$ s, which suggests that these electron-only reconnection events are individually rather short lived.

4.2. *Outflow velocity*

One can obtain an estimate of the electron outflow velocity in the reconnecting sheets by a simple scaling argument. Our configuration is a current sheet of thickness a and length $L \gg a$, and a known upstream field B_{in}. The electrons flow into the sheet at u_{in}, and out at u_{out} (which are related to ϕ via (2.11)). We will assume that $g_e = 0$ for simplicity; although this is not realistic, on the level of the scaling arguments presented here it is irrelevant.

First, because upon inspecting (2.11), $\boldsymbol{\nabla}_\perp \cdot \boldsymbol{u}_{\mathrm{eff}} = 0$,

$$L u_{\mathrm{in}} \sim a u_{\mathrm{out}}. \tag{4.4}$$

Second, because $L \gg a$, the upstream energy is dominated by the magnetic field, while the energy downstream is dominated by the ion flow and the density perturbations (Zocco & Schekochihin 2011). Balancing these,

$$\frac{B_{\mathrm{in}}^2}{8\pi} \sim \left[1 + \frac{Z}{\tau}(1 - \hat{\Gamma}_0)\right] \frac{Z}{\tau}(1 - \hat{\Gamma}_0) \frac{e^2 n_{0e}}{2T_{0e}} \phi_{\mathrm{out}}^2. \tag{4.5}$$

In the limit $\rho_i \ll a$, $Z/\tau(1 - \hat{\Gamma}_0) \approx (\rho_s/a)^2$, and using (2.11), this just results (reassuringly) in Alfvénic outflows, $u_{\mathrm{out}} \sim v_{\mathrm{A}y}$, where $v_{\mathrm{A}y} = B_{\mathrm{in}}/\sqrt{4\pi n_{0i} m_i}$. In the case where $\rho_i \gg a$, using $\hat{\Gamma}_0 \approx 0$, we find

$$u_{\mathrm{out}} \sim \sqrt{\frac{1}{2}\left(1 + \frac{Z}{\tau}\right)} v_{\mathrm{A}y} \frac{\rho_i}{a}, \tag{4.6}$$

which is just the in-plane kinetic-Alfvén wave speed. So, rather different from the MHD case, the outflow velocity depends on the thickness of the sheet. Written in terms of the electron Alfvén speed, this is

$$u_{\mathrm{out}} \sim \sqrt{\frac{\beta_i}{2}\left(1 + \frac{Z}{\tau}\right)} v_{\mathrm{A}ey} \frac{d_e}{a}. \tag{4.7}$$

https://doi.org/10.1017/S0022377819000941 Published online by Cambridge University Press

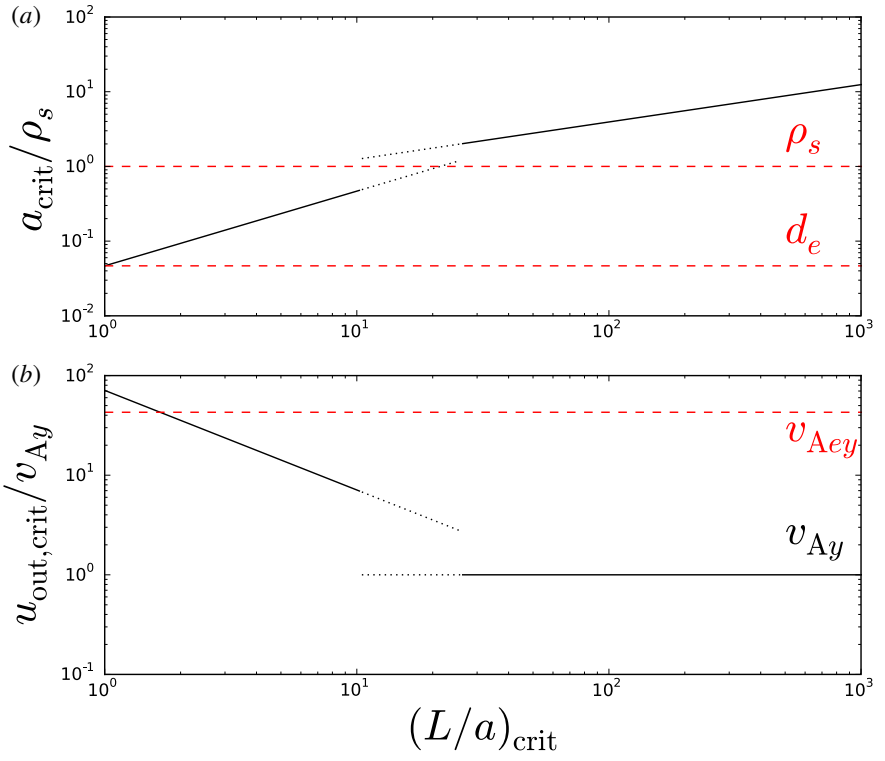

FIGURE 1. In black, the disrupted thicknesses (*a*) and outflow velocities (*b*) of reconnecting sheets as a function of aspect ratio (cf. (4.2) and (4.6)). Because we have only derived scalings in the asymptotic limits $a \gg \rho_s$ and $a \ll \rho_s$, for $0.5 < a_{\rm crit}/\rho_s < 2$ we have plotted these two scalings as dotted lines; the true scaling must lie between them. Red dashed lines show the positions of ρ_s and d_e (*a*) and $v_{{\rm A}ey}$ (*b*). We have used parameters taken from Stawarz *et al.* (2019), $\beta_e = 0.5$, $\tau = 10$.

For the Phan *et al.* (2018) sheets, our model predicts (with $\beta_i \approx 5$, cf. Stawarz *et al.* 2019) $u_{\rm out}/v_{{\rm A}ey} \approx 0.4$, while the observed outflow speed in Phan *et al.* (2018) is $u_{\rm out}/v_{{\rm A}ey} \approx 0.25 - 0.45$; given the idealisations involved (not to mention the fact that we are pushing our equations rather beyond their low-β regime of validity), this is reasonable agreement. More generally, we plot the dependence of the thickness at disruption, $a_{\rm crit}$, and the electron outflow velocity $u_{\rm out,crit}$, as functions of $(L/a)_{\rm crit}$ in figure 1.

Finally, it is worth asking what the effect of relaxing the low-β ordering of the KREHM equations would be on the tearing mode and on the critical aspect ratio we obtain here. We have shown in § 3.4 that β does not make a difference to the collapse process. Numata & Loureiro (2015) have shown that, if ρ_i/a and ρ_s/a are kept constant, the gyrokinetic tearing mode growth rate basically agrees with KREHM, i.e. proportional to $\beta_e^{-1/2}$. Thus, we believe that using the KREHM tearing mode scalings is physically (if not quite mathematically) reasonable up to $\beta_e \sim 1$.

5. Conclusions

We have developed a theoretical model for low-β current sheet formation and disruption by reconnection, and predict that sheets that are not sufficiently anisotropic

https://doi.org/10.1017/S0022377819000941 Published online by Cambridge University Press

will collapse to scales much smaller than the ion kinetic scales (ρ_s and ρ_i), only reconnecting when their thickness is a few times the electron inertial scale d_e. For such sheets, we predict electron jets with velocities an appreciable fraction of the electron Alfvén velocity (i.e. much larger than the ion Alfvén velocity), and that there will be no ion-scale region and very slow or no ion outflows. As the aspect ratio of the sheets is varied, there is a gradual transition between the usual 'ion-coupled' regime and this new regime of 'electron-only' reconnection, with sheets reconnecting at thickness $a \approx \rho_s$ when their aspect ratio $L/a \approx 10$. We find that in the magnetosheath, this means that the aspect ratio of reconnecting sheets, observed to be of thickness $a \approx 4d_e$, is no more than a factor of ≈ 4. Our results may thus help to explain recent observations of electron-only reconnection in the magnetosheath (Phan *et al.* 2018).

Our picture of reconnection onset is based on two phenomena. First, ideal current sheets tend to collapse (Syrovatskii 1981; Chapman & Kendall 1963; Biskamp 2000), and we show in § 3 that this collapse does not have to stop at the ion scale. Second, this ideal collapse process breaks down when the tearing mode growth rate becomes larger than the collapse (or sheet formation) rate, an application of the ideas of Uzdensky & Loureiro (2016) to a collisionless plasma. This implies a critical aspect ratio at which reconnection onset occurs, which we derive in § 4. Importantly, the sheet thickness at disruption can be above or below the ion scales, and so we can predict the physical conditions in which we expect ion-coupled reconnection to give way to electron-only reconnection.

Our analysis is based on the KREHM equations, which are derived from gyrokinetics for $\beta_e \sim \beta_i \sim Zm_e/m_i \ll 1$. This low-$\beta$ ordering is not usually formally valid in the magnetosheath. However, we can show that, in fact, the collapse process does not depend on the low β, and KREHM does a surprisingly good job of predicting the full gyrokinetic tearing rates even at moderate β_e. This perhaps explains why our estimates of electron outflow velocities agree reasonably well with the MMS observations. More generally, we believe that KREHM, while not always formally valid, is a useful minimal physical model of collisionless reconnection, which allows us to make theoretical progress in understanding electron-only reconnection and the transition from the ion-coupled to electron-only regimes.

Boldyrev & Loureiro (2019) use a different approach to the one used in this work: instead of studying a nonlinear collapsing solution, they show that if helicity in a structure is held constant, the nonlinear interaction is minimised by making the structure as sheet like as possible: thus, sheet-like structures last longer. They then argue that this means that the turbulence favours the creation of highly sheet-like structures, but that this is limited by the tearing instability, which then sets a particular critical aspect ratio (as does our analysis). Despite the overall similarity of the results, there are some important differences in the two pictures: in ours, the nonlinear interaction actively produces increasingly sheet-like structures, while in Boldyrev & Loureiro (2019), its role is to rapidly remove non-sheet-like structures. Our method has the advantage that it also works for sheets thicker than the ion scales, and we can therefore predict when one expects to see electron-only versus ion-coupled reconnection, depending on the characteristic aspect ratios of sheets as a function of their thickness.

In turbulence models that include the phenomenon of dynamic alignment (Boldyrev 2006; Chandran *et al.* 2015; Mallet & Schekochihin 2017), the turbulent structures at scale λ are sheet like in the perpendicular plane, with aspect ratios $\propto (\lambda/L_\perp)^{-1/4}$, where $L_\perp$ is the outer scale at which energy is injected into the system. Thus, for electron-only reconnection to be observed in turbulence, energy must be injected

https://doi.org/10.1017/S0022377819000941 Published online by Cambridge University Press

relatively close to the ion scales: in the magnetosheath, this injection could potentially come in the form of Alfvén vortices (Alexandrova 2008), perhaps driven by density gradients (Sundkvist & Bale 2008). If this picture is correct, electron-only reconnection may be relevant in other astrophysical environments with large density inhomogeneities, for example close to shocks. The appearance of electron-only reconnection in turbulent systems where the driving scale is relatively close to the ion scales has been observed rather clearly in the (two-dimensional) hybrid turbulence simulations of Califano *et al.* (2018), who observed electron-only reconnection when $d_i/L_\perp \approx 0.6$, but ion-coupled reconnection when $d_i/L_\perp \approx 0.3$. Our results therefore provide a theoretical context for these numerical results.

Another low-β_e environment of interest is the inner heliosphere and solar corona, currently being explored by the Parker Solar Probe (Fox *et al.* 2016). Our results show that whether ion-coupled or electron-only reconnection, or a mixture of the two, occur in this turbulent setting depends crucially on the length of the inertial range between the injection scale and the ion scales.

However, a detailed picture of electron-only reconnection onset in turbulence in the range of scales between ρ_s and d_e requires a model of how the aspect ratios of typical turbulent structures evolve in this range in the absence of reconnection (or, indeed, after ion-coupled reconnection decreases the typical aspect ratio, see e.g. Mallet, Schekochihin & Chandran 2017): this will be the focus of future work.

Acknowledgements

We thank A. A. Schekochihin, T. D. Phan, R. Meyrand, D. Grošelj and P. Sharma Pyakurel for useful conversations, and the anonymous reviewers for their helpful comments. This work was supported by NASA grant NNX16AP95G.

Appendix A. Steady-state reconnecting sheet

Let us perform a scaling analysis of (2.1)–(2.3), similarly to Parker (1957) and Sweet (1958), and find a steady-state reconnecting configuration. The existence of this hypothetical configuration is quite reassuring, but as we have shown in § 4, this steady-state configuration is not realisable, because it is violently unstable. This is reminiscent of the results of Loureiro, Schekochihin & Cowley (2007), Pucci & Velli (2014) and Uzdensky & Loureiro (2016) on the resistive plasmoid instability. We will work in two dimensions, i.e. $\partial/\partial z = 0$, and for simplicity set $g_e = 0$. Our configuration will the same as in § 4.2, namely a current sheet of thickness a and a length $L \gg a$, with upstream field $B_{\rm in}$, and electrons flowing into the sheet at $u_{\rm in}$, and out at $u_{\rm out}$. The analysis of (4.4)–(4.7) to determine the outflow velocity in terms of a is therefore still valid.

We additionally require a steady state, $\partial/\partial t = 0$. To achieve this, we balance the nonlinear terms in (2.2),

$$\left\{A_\parallel, \left[1 + \frac{Z}{\tau}(1 - \hat{\Gamma}_0)\right]\phi\right\} \sim \{\phi, d_e^2 \nabla_\perp^2 A_\parallel\}. \tag{A 1}$$

This gives

$$a \sim \begin{cases} d_e, & d_e \gg \rho_i, \\ \dfrac{d_e}{\sqrt{1 + Z/\tau}}, & d_e \ll \rho_i, \end{cases} \tag{A 2}$$

https://doi.org/10.1017/S0022377819000941 Published online by Cambridge University Press

using the small- and large-argument expansions of $\hat{\Gamma}_0$. Thus, these steady-state sheets have a constant thickness $a \sim d_e$, and an arbitrary length L, i.e.

$$\frac{u_{\rm in}}{u_{\rm out}} \sim \frac{d_e}{L}. \tag{A 3}$$

The dimensionless reconnection rate as usually defined is

$$R \sim \frac{u_{\rm in}}{v_{\rm Ay}} \sim \begin{cases} d_e/L, & d_e \gg \rho_i, \\ \rho_i/L, & d_e \ll \rho_i. \end{cases} \tag{A 4}$$

We have managed to derive a Sweet–Parker-like scenario for collisionless reconnection. The result for $d_e \gg \rho_i$ has been previously discovered by Wesson (1990), while Bulanov, Pegoraro & Sakharov (1992) and Avinash *et al.* (1998) also derived the scaling (A 3) for electron MHD (i.e. in the whistler frequency range).

Note that in the case $d_e \ll \rho_i$, the outflow velocity is

$$u_{\rm out} \sim \sqrt{\frac{\beta_i}{2}\left(1+\frac{Z}{\tau}\right)}\, v_{{\rm A}ey}, \tag{A 5}$$

of order the electron Alfvén velocity $v_{{\rm A}ey}$. In § 4, we show that this steady-state configuration is not realisable, because reconnection onset occurs at a somewhat larger thickness.

Appendix B. Tearing mode in a sheet with thickness below the ion scales

Let us analyse the tearing mode of (2.1)–(2.3) – we will study the two-dimensional case, $\partial/\partial z = 0$, and use as our equilibrium

$$\phi_0 = 0, \quad g_{e0} = 0, \quad A_{\parallel 0} = A_{\parallel 0}(x), \tag{B 1a–c}$$

where $A_{\parallel 0}(x)$ is controlled by a dimensionless function $f(x)$, varying on the equilibrium scale length a,

$$B_{y0} = -\frac{{\rm d}A_{\parallel 0}}{{\rm d}x} = b_a f(x). \tag{B 2}$$

Due to the symmetry of this equilibrium, our perturbations take the form

$$\left.\begin{matrix} \phi_1 \\ A_{\parallel 1} \\ g_{e1} \end{matrix}\right\} = \left\{\begin{matrix} \phi(x) \\ A_\parallel(x) \\ g_e(x) \end{matrix}\right\} {\rm e}^{{\rm i}k_y + \gamma t}. \tag{B 3}$$

We will discuss two different regimes,

$$\text{(i)} \quad a \gg \rho_s \gg d_e, \tag{B 4}$$

$$\text{(ii)} \quad \rho_s \gg a \gg d_e, \tag{B 5}$$

where (i) has already been treated by ZS11 (and references therein), while (ii) represents the tearing of sub-ion-scale sheets we are interested in the present work.

https://doi.org/10.1017/S0022377819000941 Published online by Cambridge University Press

The linearised equations may be written[8]

$$\frac{2}{d_e^2}\frac{\delta}{af}\frac{Z}{\tau}(1-\hat{\Gamma}_0)\tilde{\phi} = \left[\partial_x^2 - k_y^2 - \frac{f''}{f}\right] A_\parallel, \tag{B 6}$$

$$\frac{\delta}{af}(1-d_e^2\partial_x^2)A_\parallel = \left[1 + G\frac{Z}{\tau}(1-\hat{\Gamma}_0)\right]\tilde{\phi}, \tag{B 7}$$

where

$$\delta = \frac{\gamma a B_0}{k_y b_a v_{\mathrm{the}}}, \quad \tilde{\phi} = -\frac{c}{v_{\mathrm{the}}} i\phi, \tag{B 8a,b}$$

and the function G, which results from solving the linearised g_e equation (Zocco & Schekochihin 2011), is

$$G\left(\frac{a|f|}{\delta}\right) = -2\left[\frac{\delta^2}{a^2 f^2} + \frac{1}{Z'(i\delta/a|f|)}\right], \tag{B 9}$$

Z here being the plasma dispersion function. This has limiting values $G(0) = 3$, $G(\infty) = 1$. We will make further progress by, as usual, solving separately in an 'outer region' where $x \sim a$ and an 'inner region' where $x \ll a$.

B.1. *Outer region*

Here, $x \sim a$ and $G \approx 1$, and $\partial_x^2 \sim f''/f \sim 1/a$. We may therefore neglect $d_e^2\partial_x^2 \ll 1$ in (B 7). The structure of the equation depends on a/ρ_s. In case (i), $a \gg \rho_s$, one can expand $\hat{\Gamma}_0$ for small argument and show that the left-hand side of (B 6) is smaller than the right-hand side by γ/ω_{Ay}, where $\omega_{Ay} = k_y b_a f/\sqrt{4\pi n_{0i} m_i}$ is the in-plane Alfvén frequency; assuming this is small (which may be checked afterwards), one just obtains the same outer region equation as in the MHD tearing mode,

$$\left[\partial_x^2 - k_y^2 - \frac{f''}{f}\right] A_\parallel = 0. \tag{B 10}$$

In case (ii), however, where $a \ll \rho_s$, $\hat{\Gamma}_0 \approx 0$ and (B 7) becomes

$$\frac{\delta}{af} A_\parallel = \left[1 + \frac{Z}{\tau}\right]\tilde{\phi}. \tag{B 11}$$

Substituting this into (B 6) (again taking $\hat{\Gamma}_0 \approx 0$),

$$\lambda^2 \frac{2}{f^2}\frac{1}{\frac{\tau}{Z}+1} A_\parallel = a^2\left(\partial_x^2 - k_y^2 - \frac{f''}{f}\right) A_\parallel, \tag{B 12}$$

where $\lambda^2 = \delta^2/d_e^2$. The left-hand side may only be neglected in the outer region (where $f \sim 1$) if $\lambda^2 \ll 1$. In this case, one can see that, because $\delta B_y = -\partial_x A_\parallel$ must change sign at $x = 0$,

$$A_\parallel^{\mathrm{outer}} = A_\parallel(0)\left(1 + \frac{1}{2}\Delta'|x|\right) \quad \text{for } x \ll a. \tag{B 13}$$

We will determine when this is valid later. For $k_y a \ll 1$, $\Delta' a \propto (k_y a)^{-n}$ with $1 \leqslant n \leqslant 2$[9].

[8] Neglecting $k_y^2 d_e^2$ and $d_e^2 f''/f$ compared to unity.

[9] $n = 1$ corresponds to, for example, a 'Harris'-type equilibrium $f = \tanh(x/a)$, while an example of an $n = 2$ equilibrium is $f = \sin(x/a)$.

https://doi.org/10.1017/S0022377819000941 Published online by Cambridge University Press

B.2. *Inner region*

Here, $x \ll a$, $\partial_x^2 \gg k_y^2, f''/f$ and $f \approx x/a$. Our analysis will at first follow ZS11 exactly. The equations become

$$\frac{2}{d_e^2}\frac{\delta}{x}\frac{Z}{\tau}(1-\hat{\Gamma}_0)\tilde{\phi} = \partial_x^2 A_\parallel, \tag{B 14}$$

$$\frac{\delta}{x}(1-d_e^2\partial_x^2)A_\parallel = \left[1+G\frac{Z}{\tau}(1-\hat{\Gamma}_0)\right]\tilde{\phi}, \tag{B 15}$$

where $\hat{\Gamma}_0 = \hat{\Gamma}_0(\partial_x^2)$. Let us rescale the coordinate to $\xi = x/\delta_{\rm in}$, where $\delta_{\rm in}$ will be chosen later. Replacing the term involving $\hat{\Gamma}_0$ in (B 15),

$$\frac{2\delta\delta_{\rm in}}{d_e^2}\frac{Z}{\tau}(1-\hat{\Gamma}_0)\tilde{\phi} = \xi A_\parallel'', \tag{B 16}$$

$$\frac{A_\parallel}{\xi} - \frac{\delta_{\rm in}}{\delta}\tilde{\phi} = \frac{d_e^2}{\delta_{\rm in}^2}\left(1+\frac{\delta_{\rm in}^2}{2\delta^2}G\xi^2\right)\frac{A_\parallel''}{\xi}, \tag{B 17}$$

where primes denote derivative with respect to ξ. If one wants to include the case where $\delta_{\rm in} \sim \rho_s$, the operator $\hat{\Gamma}_0$ is difficult to deal with analytically: we will follow ZS11 and use the Padé approximant

$$\frac{Z}{\tau}\left(1-\hat{\Gamma}_0\right) \approx -\frac{\rho_s^2\partial_x^2}{1-(1/2)\rho_i^2\partial_x^2}. \tag{B 18}$$

Let us make the helpful substitution $\chi = \xi A_\parallel' - A_\parallel = \xi^2(A_\parallel/\xi)'$, so that $\chi' = \xi A_\parallel''$. Differentiating (B 17), using the approximant (B 18) in (B 16) and integrating once, the equations in terms of χ are

$$-\frac{2\delta\rho_s^2}{d_e^2\delta_{\rm in}}\tilde{\phi}' = \chi - \chi_0 - \frac{\rho_i^2}{2\delta_{\rm in}^2}\chi'', \tag{B 19}$$

$$\frac{\mathrm{d}}{\mathrm{d}\xi}\left(\frac{1}{\xi^2}+\frac{\delta_{\rm in}^2}{2\delta^2}G\right)\chi' = \frac{\delta_{\rm in}^2}{d_e^2}\frac{\chi}{\xi^2} - \frac{\delta_{\rm in}^3}{d_e^2\delta}\tilde{\phi}'. \tag{B 20}$$

Combining these two equations, we get

$$\xi^2\frac{\mathrm{d}}{\mathrm{d}\xi}\left[\frac{1}{\xi^2}+\frac{\delta_{\rm in}^2}{2\delta^2}\left(G+\frac{\tau}{Z}\right)\right]\chi' = \frac{\delta_{\rm in}^2}{\delta^2}\left[\lambda^2\chi + \frac{1}{2}\xi^2\frac{\delta_{\rm in}^2}{\rho_s^2}(\chi-\chi_0)\right]. \tag{B 21}$$

Noting that $\xi \sim 1$ in the inner region, we can compare the size of the two terms on the right-hand side.

In case (i), $a \gg \rho_s$, we must allow a finite $\delta_{\rm in}/\rho_s$ and must keep both of them. It therefore makes sense to define $\delta_{\rm in} = (\sqrt{2}\rho_s\delta)^{1/2}$, $\alpha = \delta_{\rm in}/\sqrt{2}\delta$, $\tilde{\lambda}^2 = \lambda^2\alpha^2$ and we obtain the same equations as in ZS11,

$$\xi^2\frac{\mathrm{d}}{\mathrm{d}\xi}\left[\frac{1}{\xi^2}+\frac{\alpha^2}{2}\left(G+\frac{\tau}{Z}\right)\right]\chi' = \tilde{\lambda}^2\chi + \xi^2(\chi-\chi_0). \tag{B 22}$$

https://doi.org/10.1017/S0022377819000941 Published online by Cambridge University Press

It is then possible to solve this analytically in terms of a nested 'ion inner region' and 'electron inner region', matched to each other and to the outer solution, via the matching condition

$$\frac{1}{\chi_0}\int_0^\infty \frac{\chi'}{\xi}\mathrm{d}\xi = -\frac{1}{2}\Delta'\delta_{\mathrm{in}}. \tag{B 23}$$

One can also (again, following ZS11) guess the scalings of the solution on dimensional grounds. The width of χ'/ξ in the integral above is $x\sim\delta$, or $\xi\sim 1/\alpha$. From (B 22), $\chi'/\xi \sim \tilde{\lambda}^2\chi$, whence $\tilde{\lambda}^2 \sim \Delta'\delta_{\mathrm{in}}\alpha$. For $\Delta'\delta_{\mathrm{in}} \gg 1$, the current cannot depend on Δ', and we cannot use (B 23); instead $\chi'/\xi \sim \chi$ (the current is limited by δ_{in}, $A_\parallel'' \sim A_\parallel/\delta_{\mathrm{in}}^2$), and so $\tilde{\lambda}^2 \sim \alpha$. The resulting growth rates γ, inner widths δ_{in}, and electron region widths δ are shown in table 1. The maximum growth rate, obtained by inserting $\Delta'\delta_{\mathrm{in}} \sim 1$ into the small-Δ' expression (or alternatively by balancing the small- and large-Δ' growth rates), is also shown.

One might also be interested in the dependence of the growth rates on τ/Z. It is possible to solve this equation analytically (see ZS11), showing that in fact, the growth rates are proportional to

$$H(\tau/Z) = \sqrt{1+\tau/Z}. \tag{B 24}$$

This factor is also shown in table 1.

In case (ii), $a \ll \rho_s$, there is no space for the ion inner region to form, and we must instead match the solution in the electron inner region directly onto the outer solution. Going back to (B 21), if $\delta_{\mathrm{in}} \ll \rho_s$ (as it must be since $\rho_s \gg a \gg \delta_{\mathrm{in}}$), we can neglect the second term on the right-hand side, and set $\delta_{\mathrm{in}} = \delta$, obtaining

$$\xi^2\frac{\mathrm{d}}{\mathrm{d}\xi}\left[\frac{1}{\xi^2}+\frac{1}{2}\left(G+\frac{\tau}{Z}\right)\right]\chi' = \lambda^2\chi. \tag{B 25}$$

We can again guess the scalings on dimensional grounds, similarly to case (i). For $\Delta'\delta \ll 1$, $\lambda^2 \sim \Delta'\delta$. Therefore, we may solve (B 25) perturbatively in powers of $\lambda^2 \ll 1$, to first order, i.e. $\chi = \chi_0 + \chi_1$, with the boundary condition that the current χ'/ξ is even as $\xi \to 0$. Setting the right-hand side to zero, the zeroth-order solution χ_0 is just a constant. This means our solution is equivalent to taking a 'constant-ψ' approximation (Furth, Killeen & Rosenbluth 1963). At the next order, using χ_0 on the right-hand side and the boundary condition, we obtain

$$\frac{\chi_1'}{\xi} = -\frac{\lambda^2\chi_0}{1+\xi^2/2(G+\tau/Z)}, \tag{B 26}$$

and matching this to the outer solution using (B 23),

$$\lambda^2 = \frac{\Delta'\delta}{2I}, \tag{B 27}$$

where

$$I = \int_0^\infty \frac{\mathrm{d}\xi}{1+\xi^2/2(G+\tau/Z)}. \tag{B 28}$$

This is precisely the same growth rate, including the prefactor, as for the small-Δ' case with $a \gg \rho_s$ (cf. Zocco & Schekochihin (2011), equation B71). For $\tau/Z \gg 1$, we can neglect G and $I \sim \sqrt{Z/\tau}$, while for $\tau/Z \ll 1$, $I \sim 1$. We include this effect in table 1 by amending the scalings by the factor $H(\tau/Z)$ defined in (B 24).

https://doi.org/10.1017/S0022377819000941 Published online by Cambridge University Press

For $\Delta'\delta \gg 1$, on dimensional grounds, $\lambda^2 \sim 1$: unfortunately, this invalidates the neglect of the left-hand side in (B 12), meaning that our matching condition (B 23) is no longer valid. We have not yet obtained an analytic solution to the equations in this case. However, since on physical grounds the growth rate must decrease as $k_y \to 0$, it is reasonable to assume that the maximum growth rate of the tearing mode may be estimated by setting $\Delta'\delta \sim 1$ in the scalings obtained for the $\Delta'\delta \ll 1$ limit. The scalings derived here for the tearing mode with $a \ll \rho_s$ are also shown in table 1.

Boldyrev & Loureiro (2019) have derived a somewhat similar tearing mode for the 'inertial kinetic-Alfvén' regime (Chen & Boldyrev 2017). The difference between their equations and the KREHM equations (Zocco & Schekochihin 2011) is that theirs are fluid (i.e. they do not contain heating), and, secondly, they order $\beta_i \sim 1$, which introduces an additional term in our (B 16) (their equation 18) proportional to $\beta_i\phi''$ (b_z'' in their variables). This means they can neglect the term on the right-hand side in our equation, because in the inner region the gradients are large, and then makes their equations structurally identical to the MHD tearing equations. They therefore obtain different maximum growth rates $\gamma_{\max} \sim (d_e/a)^{1+1/n} v_{\mathrm{A}ey}/a$ that are a multiplied by a factor $\beta_i^{1/2}$ compared to ours.

REFERENCES

ALEXANDROVA, O. 2008 Solar wind versus magnetosheath turbulence and Alfvén vortices. *Nonlin. Proc. Geophys.* **15**, 95.

AVINASH, K., BULANOV, S. V., ESIRKEPOV, T., KAW, P., PEGORARO, F., SASOROV, P. V. & SEN, A. 1998 Forced magnetic field line reconnection in electron magnetohydrodynamics. *Phys. Plasmas* **5** (8), 2849–2860.

BISKAMP, D. 2000 *Magnetic Reconnection in Plasmas*. Cambridge University Press.

BOLDYREV, S. 2006 Spectrum of magnetohydrodynamic turbulence. *Phys. Rev. Lett.* **96**, 115002.

BOLDYREV, S. & LOUREIRO, N. F. 2019 Role of reconnection in inertial kinetic-Alfvén turbulence. *Phys. Rev. Research*, doi:10.1103/PhysRevResearch.1.012006.

BULANOV, S. V., PEGORARO, F. & SAKHAROV, A. S. 1992 Magnetic reconnection in electron magnetohydrodynamics. *Phys. Fluids* B **4** (8), 2499–2508.

CALIFANO, F., CERRI, S. S., FAGANELLO, M., LAVEDER, D. & KUNZ, M. W. 2018 Electron-only magnetic reconnection in plasma turbulence. arXiv:1810.03957.

CHANDRAN, B. D. G., SCHEKOCHIHIN, A. A. & MALLET, A. 2015 Intermittency and alignment in strong RMHD turbulence. *Astrophys. J.* **807**, 39.

CHAPMAN, S. & KENDALL, P. C. 1963 Liquid instability and energy transformation near a magnetic neutral line: a soluble non-linear hydromagnetic problem. *Proc. R. Soc. Lond.* A **271**, 435–448.

CHEN, C. H. K. & BOLDYREV, S. 2017 Nature of kinetic scale turbulence in the Earth's magnetosheath. *Astrophys. J.* **842**, 122.

DEL SARTO, D., PUCCI, F., TENERANI, A. & VELLI, M. 2016 'Ideal' tearing and the transition to fast reconnection in the weakly collisional MHD and EMHD regimes. *J. Geophys. Res. (Space Physics)* **121**, 1857–1873.

FOX, N. J., VELLI, M. C., BALE, S. D., DECKER, R., DRIESMAN, A., HOWARD, R. A., KASPER, J. C., KINNISON, J., KUSTERER, M., LARIO, D. *et al.* 2016 The Solar Probe Plus mission: humanity's first visit to our star. *Space Sci. Rev.* **204**, 7.

FURTH, H. P., KILLEEN, J. & ROSENBLUTH, M. N. 1963 Finite-resistivity instabilities of a sheet pinch. *Phys. Fluids* **6**, 459–484.

GROŠELJ, D., CERRI, S. S., BAÑÓN NAVARRO, A., WILLMOTT, C., TOLD, D., LOUREIRO, N. F., CALIFANO, F. & JENKO, F. 2017 Fully kinetic versus reduced-kinetic modeling of collisionless plasma turbulence. *Astrophys. J.* **847**, 28.

https://doi.org/10.1017/S0022377819000941 Published online by Cambridge University Press

JAIN, N., VON STECHOW, A., MUÑOZ, P. A., BÜCHNER, J., GRULKE, O. & KLINGER, T. 2017 Electron-magnetohydrodynamic simulations of electron scale current sheet dynamics in the vineta. II guide field reconnection experiment. *Phys. Plasmas* **24** (9), 092312.

JI, H., ALT, A., ANTIOCHOS, S., BAALRUD, S., BALE, S., BELLAN, P. M., BEGELMAN, M., BERESNYAK, A., BLACKMAN, E. G., BRENNAN, D. *et al.* 2019 Major Scientific Challenges and Opportunities in Understanding Magnetic Reconnection and Related Explosive Phenomena throughout the Universe. In *Bulletin of the American Astronomical Society*, BAAS, vol. 51, p. 5.

LOUREIRO, N. F., SCHEKOCHIHIN, A. A. & COWLEY, S. C. 2007 Instability of current sheets and formation of plasmoid chains. *Phys. Plasmas* **14** (10), 100703.

MALLET, A. & SCHEKOCHIHIN, A. A. 2017 A statistical model of three-dimensional anisotropy and intermittency in strong alfvénic turbulence. *Mon. Not. R. Astron. Soc.* **466**, 3918.

MALLET, A., SCHEKOCHIHIN, A. A. & CHANDRAN, B. D. G. 2017 Disruption of Alfvénic turbulence by magnetic reconnection in a collisionless plasma. *J. Plasma Phys.* **83** (6), 905830609.

MANDT, M. E., DENTON, R. E. & DRAKE, J. F. 1994 Transition to whistler mediated magnetic reconnection. *Geophys. Res. Lett.* **21**, 73–76.

NUMATA, R. & LOUREIRO, N. F. 2015 Ion and electron heating during magnetic reconnection in weakly collisional plasmas. *J. Plasma Phys.* **81**, 305810201.

PARKER, E. N. 1957 Sweet's mechanism for merging magnetic fields in conducting fluids. *J. Geophys. Res.* **62**, 509–520.

PHAN, T. D., EASTWOOD, J. P., SHAY, M. A., DRAKE, J. F., SONNERUP, BU. Ö., FUJIMOTO, M., CASSAK, P. A., ØIEROSET, M., BURCH, J. L., TORBERT, R. B. *et al.* 2018 Electron magnetic reconnection without ion coupling in earths turbulent magnetosheath. *Nature* **557** (7704), 202.

PUCCI, F. & VELLI, M. 2014 Reconnection of quasi-singular current sheets: the 'ideal' tearing mode. *Astrophys. J. Lett.* **780**, L19.

ROGERS, B. N., DENTON, R. E., DRAKE, J. F. & SHAY, M. A. 2001 Role of dispersive waves in collisionless magnetic reconnection. *Phys. Rev. Lett.* **87**, 195004.

SCHEKOCHIHIN, A. A., COWLEY, S. C., DORLAND, W., HAMMETT, G. W., HOWES, G. G., QUATAERT, E. & TATSUNO, T. 2009 Astrophysical gyrokinetics: kinetic and fluid turbulent cascades in magnetized weakly collisional plasmas. *Astrophys. J. Supp.* **182**, 310.

SHARMA PYAKUREL, P., SHAY, M. A., PHAN, T. D., MATTHAEUS, W. H., DRAKE, J. F., TENBARGE, J. M., HAGGERTY, C. C., KLEIN, K., CASSAK, P. A., PARASHAR, T. N. *et al.* 2019 Transition from ion-coupled to electron-only reconnection: basic physics and implications for plasma turbulence. *Phys. Plasmas*, doi:10.1063/1.5090403.

STAWARZ, J. E., EASTWOOD, J. P., PHAN, T. D., GINGELL, I. L., SHAY, M. A., BURCH, J. L., ERGUN, R. E., GILES, B. L., GERSHMAN, D. J., LE CONTEL, O. *et al.* 2019 Properties of the turbulence associated with electron-only magnetic reconnection in Earth's magnetosheath. *Astrophys. J. Lett.* **877**, L37.

STRAUSS, H. R. 1976 Nonlinear, three-dimensional magnetohydrodynamics of noncircular tokamaks. *Phys. Fluids* **19**, 134.

SUNDKVIST, D. & BALE, S. D. 2008 Characteristic parameters of drift vortices coupled to Alfvén waves in an inhomogeneous space plasma. *Phys. Rev. Lett.* **101**, 065001.

SWEET, P. A. 1958 The neutral point theory of solar flares. In *Electromagnetic Phenomena in Cosmical Physics* (ed. B. Lehnert), IAU Symposium, vol. 6, p. 123. CUP.

SYROVATSKII, S. I. 1981 Pinch sheets and reconnection in astrophysics. *Annu. Rev. Astron. Astrophys.* **19** (1), 163–227.

TENERANI, A., VELLI, M., PUCCI, F., LANDI, S. & RAPPAZZO, A. F. 2016 Ideally unstable current sheets and the triggering of fast magnetic reconnection. *J. Plasma Phys.* **82** (5), 535820501.

UZDENSKY, D. A. & LOUREIRO, N. F. 2016 Magnetic reconnection onset via disruption of a forming current sheet by the tearing instability. *Phys. Rev. Lett.* **116** (10), 105003.

WESSON, J. A. 1990 Sawtooth reconnection. *Nucl. Fusion* **30** (12), 2545.

WHITE, R. L., HAZELTINE, R. D. & LOUREIRO, N. F. 2018 Symmetries of a reduced fluid-gyrokinetic system. *J. Plasma Phys.* **84** (2), 905840204.

YAMADA, M., KULSRUD, R. & JI, H. 2010 Magnetic reconnection. *Rev. Mod. Phys.* **82**, 603–664.

ZOCCO, A. & SCHEKOCHIHIN, A. A. 2011 Reduced fluid-kinetic equations for low-frequency dynamics, magnetic reconnection, and electron heating in low-beta plasmas. *Phys. Plasmas* **18**, 102309.

ZWEIBEL, E. G. & YAMADA, M. 2009 Magnetic reconnection in astrophysical and laboratory plasmas. *ARA&A* **47**, 291–332.